Chapter 14

Biosensor Imaging in Brain Slice Preparations

Marina Polito, Pierre Vincent, and Elvire Guiot

Abstract

Cyclic-AMP dependent protein kinase (PKA) is present in most branches of the animal kingdom, and is an example in the nervous system where a kinase effector integrates the cellular effects of various neuromodulators. The recent development of FRET-based biosensors, such as AKAR, now allows the direct measurement of PKA activation in living cells by simply measuring the ratio between the fluorescence emission at the CFP and YFP wavelengths upon CFP excitation. This novel approach provides data with a temporal resolution of a few seconds at the cellular and even subcellular level, opening a new avenue of understanding the integration processes in space and time.

Our protocol has been optimized to study morphologically intact mature neurons and we describe how simple and cheap wide-field imaging, as well as more elaborate two-photon imaging, allows real-time monitoring of PKA activation in pyramidal cortical neurons in neonate rodent brain slices. In addition, many practical details presented here also pertain to image analysis in other cellular preparations, such as cultured cells. Finally, this protocol can also be applied to the various other CFP-YFP-based FRET biosensors that are available for other kinases or other intracellular signals. It is likely that this kind of approach will be generally applicable to a broad range of assays in the near future.

Key words Protein kinase A, Biosensor, FRET, Time-lapse imaging, Fluorescence, Brain slice preparation

1 Introduction

The cyclic adenosine monophosphate (cAMP) and protein kinase A (PKA) signaling pathway is involved in virtually all physiological processes. More specifically in the nervous system, the cAMP/PKA cascade plays an important role in several integrated brain functions, such as neuronal survival, axonal regeneration, memory and cognitive functions. At the cellular level, the cAMP/PKA cascade is responsible for the modulation of various processes, including some specific forms of synaptic plasticity, control of excitability, regulation of nuclear factors and imprinting of long-term changes. One major target of cAMP is PKA, hence the importance of monitoring its activation. Besides PKA, cAMP also directly modulates other downstream effectors, such as the exchange proteins directly

Jin Zhang et al. (eds.), *Fluorescent Protein-Based Biosensors: Methods and Protocols*, Methods in Molecular Biology, vol. 1071,
DOI 10.1007/978-1-62703-622-1_14, © Springer Science+Business Media, LLC 2014

activated by cAMP (Epac1 and Epac2) and several channels, like cyclic-nucleotide gated channels and I_h.

The cAMP/PKA signal, like many other cellular signals, takes place in the complex multidimensional space of the living cell. The temporal dimension is obviously a critical one, as the PKA signal rises following a stimulus and then declines over time as the stimulus is removed and/or feedback mechanisms cause the signal to revert towards baseline. The spatial dimension also plays a role since the concentration of signaling molecules decreases with distance. Protein-protein interactions, such as those mediated by AKAPs, maintain all partners of the signaling cascade in close proximity in so-called signaling microdomains [1]. In addition to these factors, the geometry of the cell can affect signal integration, with a high surface to volume ratio favoring the accumulation of cAMP and the activation of PKA in thin dendrites versus the cell body [2]. Therefore, since temporal and spatial measurements are of critical importance to the understanding of intracellular signaling, direct imaging of the cAMP/PKA signaling cascade is a highly desirable approach.

The first attempts to image changes in cAMP concentration in neurons made use of purified PKA chemically labeled with fluorescein and rhodamine: the dissociation of the regulatory and catalytic subunit upon cAMP binding was monitored as a decrease in fluorescence resonance energy transfer (FRET) between the two chromophores [3]. This method allowed the recording of cAMP diffusion in giant Aplysia neurons [4], then in the intact stomatogastric ganglion of the spiny lobster [5]. However, this first biochemical sensor remained impractical to use in vertebrate neurons because the recombinant and labeled holoenzyme had to be introduced into the cells of interest, a difficult task for vertebrate neurons [6]. A major breakthrough in this field resulted from the creation of FRET-based genetically encoded optical sensors, the first sensors being designed to report calcium [7, 8], eventually leading to sensors for various other biological signals.

Single wavelength sensors have been made which use the intrinsic sensitivity of GFP to pH or chloride, a property amplified by mutating the GFP sequence. They can also have an external sensor grafted to it, such as for the GCamp series of calcium biosensors. However, changes in fluorescence emission measured at a single wavelength can result from various artifacts, technical (fluctuations in illumination intensity, focus drift) or related to the cell (changes in cell volume, hence sensor concentration in the imaged volume) and this is where ratiometric quantification comes in handy. The principle of ratiometric quantification was initially demonstrated for calcium imaging using the small molecule indicator, fura2 [9]. In these studies, the measurement is done simultaneously at two wavelengths where the intensity change of the

indicator goes in the opposite direction of the biological signal of interest (i.e., intracellular calcium). Importantly, since artifactual changes affect both wavelengths by the same factor, they are cancelled in the ratio. This quantification method also applies to most FRET-based biosensors.

FRET-based biosensors are commonly constituted of a domain sensitive to the biological signal of interest sandwiched between a pair of fluorophores, usually CFP and YFP or their close derivatives [10]. The signal triggers a conformational change of the biosensor, modifying the extent of FRET from CFP to YFP upon CFP excitation, leading to reciprocal changes in the CFP and YFP fluorescence intensities. The last decade has seen the creation of a number of biosensors based on this design for biological signals ranging from the detection of the neurotransmitter glutamate [11, 12] to the monitoring of apoptosis [13]. After the original CFP-YFP pair, new fluorophores are progressively being used, resulting in improved ratio changes [14–16]. In this chapter, we will focus on one series of biosensors specifically developed to monitor PKA-mediated phosphorylation events.

A-kinase activity reporter (AKAR) is a recombinant protein composed of a phosphoamino acid binding domain and a PKA-specific substrate fused between CFP and YFP. When phosphorylated by PKA, intramolecular binding of the substrate by the phosphoamino acid binding domain drives a conformational reorganization, leading to an increase in FRET between CFP and YFP. Variants with increasingly better signals were produced over the years and are reviewed in [17]. Briefly, AKAR2.2, which employs a monomeric version of enhanced CFP (ECFP) as the donor and a monomeric version of the YFP variant, Citrine, as an acceptor, exhibits a ~25 % ratio change upon PKA phosphorylation [18]. Meanwhile, AKAR3, in which Citrine is replaced by a circularly permuted form of Venus (cpV E172), exhibits a ~40 % ratio change [19]. Finally, replacing ECFP with Cerulean led to AKAR4, with ratio changes up to 68 % [20].

Although commonly dubbed “PKA sensors”, one must keep in mind that the phosphorylation level of the biosensor results from the equilibrium between PKA-dependent phosphorylation and dephosphorylation performed by various phosphatases. An increase in AKAR signal can therefore result either from an activation of PKA, or from an inhibition of phosphatases in the context of a tonic PKA activity. This has been observed experimentally in neurons in brain slices where Gs-coupled receptors, as well as phosphatase inhibition, led to an increase in the extent of AKAR phosphorylation [21]. Since the ratio recovered slowly after agonist removal [21], one can assume that the kinetics of phosphatase-mediated dephosphorylation was much slower than that of PKA-mediated phosphorylation. Therefore, as long as

this condition is verified, one can assume that AKAR primarily reports PKA activity.

AKAR thus opened the possibility of quantifying the relative amplitude of the PKA signal obtained in different situations. For example, we measured the response to different neuropeptides, reporting a relative order of potency of the receptors CRF1 ≅ PAC1 > VPAC1 in their ability to activate the cAMP/PKA signaling cascade in pyramidal cortical neurons [22]. AKAR imaging also provided key experimental data in the temporal and spatial dimensions: by comparing AKAR response kinetics (indicating PKA activation in the bulk cytosol) with the downstream effects of PKA using electrophysiological approaches (which report PKA activation beneath the membrane), we demonstrated that neurons have a sub-membrane domain where full PKA activation occurs in ~30 s, whereas it takes 2.5 min (5× longer) to reach the maximum phosphorylation level in the bulk cytosol [21]. The potential of optical biosensors for spatial resolution was later used in combination with two-photon microscopy, revealing that cAMP accumulates in dendrites of small diameter while its concentration fades away in the bulk cytosol, an effect which most likely results from a higher surface to volume ratio in small dendrites, favoring cAMP concentration buildup [23]. Although this had been predicted theoretically [2], imaging provided a clear experimental confirmation of the importance of cell geometry on signal integration.

The spatial dimension can also be accessed using targeting domains to target the probe towards a specific subcellular compartment. AKAR2.2 fused with a nuclear localization signal at its C-terminal was thus used to monitor the kinetics of PKA activation inside the nucleus of neurons in brain slices, and reported a much slower response than in the cytosol [21].

As described above, the spatial organization of the cell of interest directly determines signal integration processes. The biological preparation is therefore an important point, particularly in the case of neurons. Our choice has been to study mature neurons in their most physiological context, i.e., in brain slice preparations made from rodent neonates. This preparation, derived from the work of electrophysiologists, has the advantage of providing morphologically intact differentiated neurons, which maintain functional network connections and bear endogenous receptors. This chapter describes the details of AKAR imaging in brain slices, emphasizing some technical points like image acquisition and image analysis. Most of the information presented here also pertains to imaging in any other preparation, including cell cultures, and potentially to many other dual-emission biosensors.

2 Materials

2.1 Solutions

1. Cutting solution contains: 125 mM NaCl, 0.4 mM $CaCl_2$, 1 mM $MgCl_2$, 1.25 mM NaH_2PO_4, 26 mM $NaHCO_3$, and 25 mM glucose, saturated with 5 % CO_2 and 95 % O_2 (*see* **Note 1**).
2. Culture medium is made of 50 % Minimum Essential Medium, 50 % Hanks' Balanced Salt Solution, 6.5 g/L glucose, penicillin–streptomycin.
3. Recording solution contains: 125 mM NaCl, 0.4 mM $CaCl_2$, 1 mM $MgCl_2$, 1.25 mM NaH_2PO_4, 26 mM $NaHCO_3$, and 25 mM glucose, saturated with 5 % CO_2 and 95 % O_2.
4. A 10× stock solution of 1.25 M NaCl, 12.5 mM NaH_2PO_4, 260 mM $NaHCO_3$ is made weekly and kept at 4 °C. On the day of the experiment, a 1× solution is prepared by diluting the stock and adding $CaCl_2$, $MgCl_2$, and glucose to the final concentrations indicated above.

2.2 Brain Slice Preparation

Brain slices are prepared from young rodents, rats at postnatal age P10 to P14, or mice at P8-P12 (*see* **Note 2**). Brain slices are cut using a vibrating blade microtome VT1200S (Leica). Brain slices are kept on a Millicell-CM membrane PICM0RG50 (Millipore).

2.3 Biosensor and Viral Vectors

1. PKA-sensitive AKAR biosensors, as well as a control version of the AKAR2.2 sensor with a T391A point mutation in the phosphorylation site, were provided by Jin Zhang, Johns Hopkins School of Medicine, Baltimore, USA.
2. The viral vector used in our experiments is derived from the Sindbis virus [24] and provided by Invitrogen, San Diego, CA. The coding sequence of the biosensor was sub-cloned into the viral vector, pSinRep5. Viral particles are produced following the guidelines published by Invitrogen.

2.4 Wide-Field Imaging

The imaging setup uses an upright microscope (Olympus BX51WI) equipped with a 20× 0.5 NA, a 40× 0.8 NA, or a 60× 0.9 NA water-immersion objective with a piezoelectric device (P-721 PIFOC, Physik Instrumente GmbH) to remotely control image focus. Epifluorescence is excited using a halogen light source, a shutter (Uniblitz, Vincent and Associates), and a D436/20 filter for excitation (*see* **Note 3**). A 455DCXT dichroic mirror separates the emission from the excitation. The emitted light is filtered by alternating the emission filters, HQ480/40 for CFP and D535/40 for YFP, with a filter wheel (Sutter Instruments, Novato, CA, USA). Filters were obtained from Chroma Technology (Brattleboro, VT, USA) or Semrock (Rochester, NY, USA). Images are recorded with a low noise CCD camera (ORCA-AG, Hamamatsu). Images for shading

correction are acquired using a 100 μM solution of Coumarin 343 in a 10 mM sodium phosphate buffer at pH 7, stored in small aliquots and kept at −20 °C (*see* **Note 4**).

2.5 Spectral Analysis

Emission spectra of the biosensor were recorded over a single neuron in the brain slice using a fibered spectrometer USB2000 (Ocean Optics) with a 600 μm fiber placed at the focal image plane of the microscope. The objective was 20× 0.5 N.A.

2.6 Two-Photon Imaging

Two-photon images were obtained with a custom-built two-photon laser scanning microscope based on an Olympus BX51WI upright microscope with a 60× 0.9 NA water-immersion objective and a Ti:sapphire laser (MaiTai HP; Spectra Physics, Mountain View, CA) tuned to 850 nm wavelength and 12 mW power for CFP excitation. Galvanometric scanners (model 6210, Cambridge Technology, Cambridge, MA) were used for raster scanning, and a piezo-driven objective scanner (P-721 PIFOC, Physik Instrumente GmbH) was used to control the depth of the focal plane in the preparation. A two-photon emission filter was used to reject residual excitation light (E700 SP, Chroma Technology, Brattleboro, VT, USA). A fluorescence cube containing 479/40 and 542/50 emission filters and a 506 nm dichroic beamsplitter (FF01-479/40, FF01-542/50, and FF506-Di02-25×36 Brightline Filters, Semrock, Rochester, NY, USA) was used for the orthogonal separation of the two fluorescence signals. Two imaging channels (H9305 photomultipliers, Hamamatsu) were used for simultaneous detection of the two types of fluorescence emission.

2.7 Image Acquisition

The wide-field imaging setup is controlled using iVision-Mac software (BioVision technologies, Exton, USA) and custom scripts. The two-photon imaging system is controlled by MPscope software [25].

2.8 Image Analysis

Image analysis is performed using Igor software (Wavemetrics, USA) and custom-written functions.

3 Methods

3.1 Brain Slice Preparation

The animal is killed by decapitation, following the guidelines of our institution. The brain is quickly removed and placed in ice-cold cutting solution. After cutting, brain slices are left for 1 h to recover in cutting solution. The Millicell membrane is placed into a 35 mm petri dish containing 1 ml of culture medium and incubated for 1 h at 35 °C in 5 % CO_2 atmosphere (*see* **Note 5**). Two to three brain slices are carefully placed onto the Millicell membrane and all cutting solution is delicately removed. The slices are then left for 1 h in the incubator before infection with a viral vector encoding the

appropriate AKAR biosensor. Viral infection is performed by gently spreading 1–3 μl of virus suspension over the surface of the brain slice with a pipette. The dish is then kept overnight in the incubator.

The next day, 1 ml of recording solution is placed on the Millicell membrane and the brain slices are gently detached and transferred into a 100 ml beaker containing recording solution gassed with 95 % O_2/5 % CO_2. Slices are left for 1 h in this solution, a time needed to recover a pH/metabolic equilibrium (*see* **Note 6**).

The imaging chamber on the microscope is continuously perfused with the recording solution saturated with 95 % O_2/5 % CO_2 at a rate of 2 ml/min. Smoothly switching between different reservoirs allows the bathing solution to be changed to a solution containing drugs without mechanically disturbing the preparation.

3.2 Wide-Field Imaging

Images (one for each CFP and YFP channel) are acquired with an exposure duration of 0.2–1 s, depending on the preparation expression level, illumination power and camera sensitivity. Image pairs are recorded at time intervals from 5 s to several minutes, depending on the duration of the biological event to be monitored (*see* **Note 3**). Besides lateral drift of the brain slice, which can be easily corrected off-line (*see* below), focus drift must be corrected in real time.

3.3 Two-Photon Imaging

CFP and YFP signals are recorded simultaneously during the scanning of the preparation by the laser beam. 512 × 512 pixels images are acquired at a rate of 1.6 frames/s. Vertical stacks of ~50 images are recorded with a 0.5 μm increment step.

For both wide-field and two-photon imaging, a total number of 100 data points with negligible photobleaching over a 1–2 h time period is common practice.

3.4 Image Analysis (Fig. 1)

Images saved by the acquisition software are immediately processed by the analysis program and the resulting ratio measurements and pseudo-color images are displayed in real time. Image analysis comprises a series of steps, based on the description made for ratiometric calcium imaging [26]:

1. Subtract the camera offset from each image.
2. Divide the intensity values by the exposure time.
3. Divide each image by the shading image of the corresponding imaging channel (*see* **Note 4**).
4. Subtract an optional background value from the image. Since the autofluorescence of the neurons is usually low compared to the fluorescence of the biosensor, and since this value cannot be determined objectively, this parameter is usually left null.
5. Correct the images for preparation movements, typically horizontal translations of several microns (*see* **Note 7**).

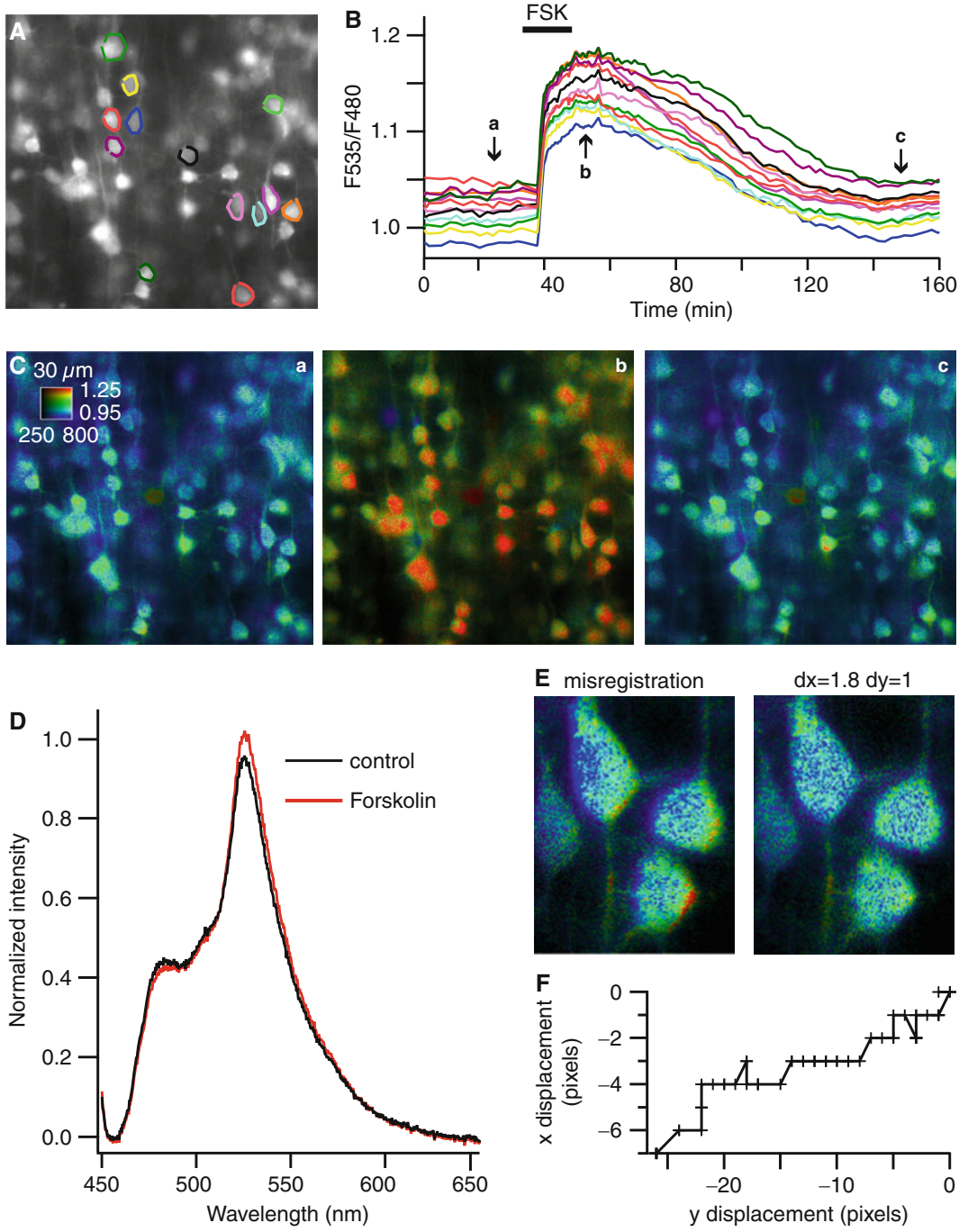

Fig. 1 Monitoring PKA activity in cortical neurons expressing AKAR2.2 by wide-field microscopy. (**a**) Fluorescence image of the brain slice expressing AKAR2.2 at 535 nm emission wavelength. (**b**) F535/F480 ratio values during the course of the recording, measured over the regions of interest of the same color and drawn on (**a**). 13 μM forskolin (FSK) was added to the bath for the time period indicated by the bar. *Arrows* indicate the time corresponding to the pseudocolor images in (**c**). (**c**) Pseudocolor images representing the F535/F480 emission ratio in control condition (*a*), in the presence of 13 μM FSK (*b*), after recovery (*c*). The calibration square indicates fluorescence intensity horizontally and the F535/F480 ratio vertically. (**d**) AKAR2.2 emission spectrum

6. Correct the images for misregistration, usually by less than 2 pixels (*see* **Note 8**).
7. Calculate the ratio pixel by pixel as Ratio = (YFP)/(CFP), using the YFP and CFP images at the two wavelengths, after the corrections described above.
8. Display the images in pseudocolor, coding the ratio value in hue and the fluorescence in intensity (*see* **Note 9**).
9. Add a calibration scale to the image. Since pseudocolor images represent two dimensions (ratio and intensity), the calibration becomes a square, showing the intensity of the pixel (in counts per pixel per second) on the horizontal axis and the ratio on the vertical axis. The size of this calibration square also defines the size scale of the image.
10. Use the regions of interest drawn on the image to calculate the average ratio as an average weighted by the intensity (*see* **Note 10**).
11. There are sometimes nonlinear deformations within the brain slice, resulting in movements which cannot be corrected by a global translation. Fine local adjustments of the regions of interest compensate for these small distortions.

3.5 Controls

CFP and YFP are far from ideal chromophores and both exhibit pH and environment sensitivities. It is therefore quite useful to check that the ratio changes recorded in an experiment are not artifactual. A control biosensor mutated in the phosphorylation site must report no ratio change in the same situation as the experiment and thus demonstrates that the ratio signal indeed reflects a phosphorylation event. The T391A mutant of AKAR2.2 is used systematically to check for a lack of ratio response in the experimental conditions of interest. The mutant biosensor also shows that cell to cell differences in ratio are not the consequence of different PKA activation level but are intrinsic to the biosensor (*see* **Note 11**) (Fig. 2).

3.6 Targeting the Biosensor to a Specific Subcellular Compartment

The fusion of a targeting domain to the biosensor allows for precise subcellular targeting into a specific cell compartment. For instance, a nuclear localization signal (NLS) fused to AKAR2 allows for the measurement of PKA activation in the nucleus [21] (Fig. 3).

Targeting the biosensor to the membrane has also been accomplished in a variety of cultured cells [20].

Fig. 1 (continued) recorded on an individual neuron in control condition and 15 min after bath application of 13 μM forskolin. (**e**) Magnification of cell bodies showing the effect of a misregistration between the F535 and F480 channels (*left*) and the corrected image (*right*). Misregistered ratio images display the characteristic "rainbow" appearance, with one edge with low ratio while the opposite edge has high ratio. The correction is calculated at the 1/5th pixel resolution. (**f**) Movement of the brain slice that occurred during the time course of the experiment

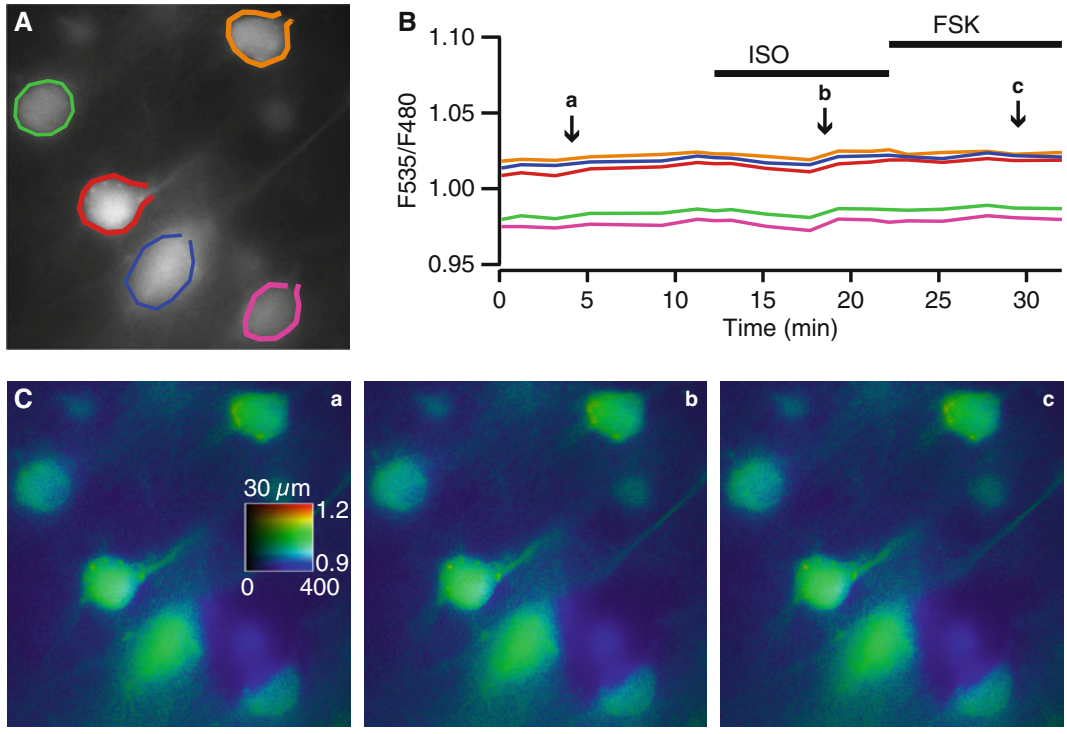

Fig. 2 Lack of response when the phosphorylation site of AKAR2.2 is mutated. (**a**) Fluorescence image of the brain slice expressing AKAR2.2mut (T391A) viewed by wide-field microscopy at the 535 nm emission wavelength. (**b**) Ratio values during the course of the recording, measured over the regions of interest of the same color and drawn on (**a**). 1 μM isoproterenol (ISO) and 13 μM forskolin (FSK) were applied in the bath for the durations indicated by the bars on the graph. *Arrows* indicate the time corresponding to the images in (**c**). (**c**) Pseudocolor images in control condition (*a*), in the presence of 1 μM isoproterenol (*b*), and in the presence of 13 μM forskolin (*c*). The calibration square indicates fluorescence intensity horizontally and F535/F480 ratio vertically

3.7 Monitoring cAMP with Epac-Based Biosensors

There are several biosensors for cAMP with slightly differing properties and a rather similar affinity for cAMP in the micromolar range [27–29]. More recently, a cAMP biosensor containing a cAMP binding pocket with increased affinity (~0.3 μM) was derived [30]. Sequential use of such biosensors allows for a rough estimate of the concentration range of cAMP reached during a given cellular response. In pyramidal cortical neurons, Epac1-camps, with micromolar affinity, shows no response to a β-adrenergic stimulation, while the Epac2-camps300, with 0.3 μM affinity shows a small but clear response (Fig. 4, from ref. 23). The sensitivity difference between these two sensors is also visible during the forskolin response, which almost saturates with Epac2-camps300 while it is only half of the maximum with Epac1-camps (Fig. 4).

3.8 Two-Photon Imaging

Two-photon image acquisition and image analysis is performed in a manner similar to wide-field imaging with the following differences: (1) laser scanning provides images that are intrinsically registered,

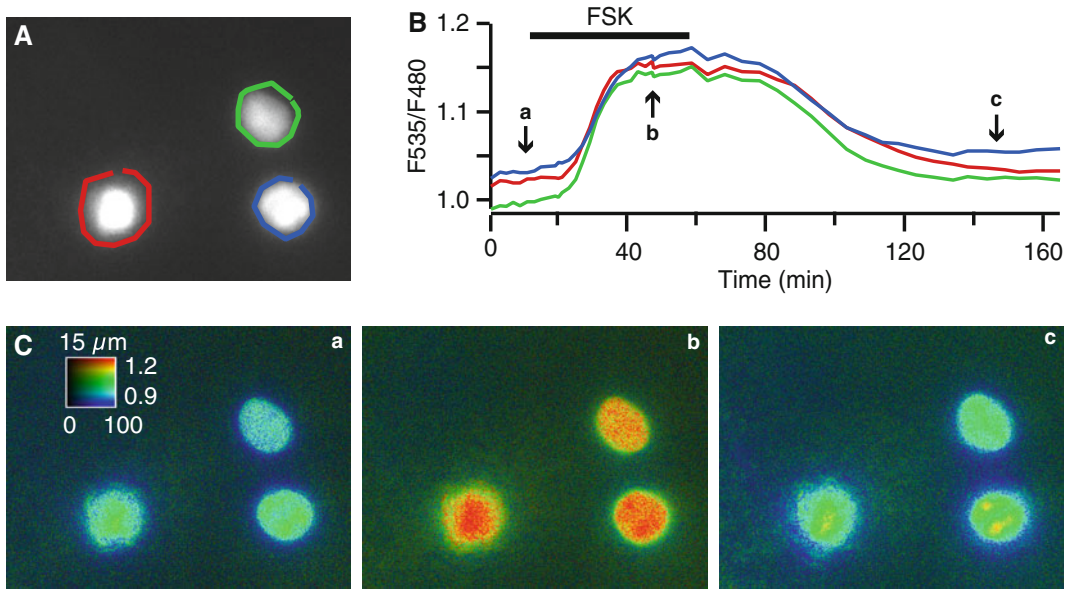

Fig. 3 Wide-field imaging of the PKA activity inside the nucleus of cortical neurons expressing AKAR2-NLS. (**a**) Fluorescence image of the brain slice at 535 nm emission wavelength. (**b**) F535/F480 ratio values during the course of the recording, measured over the regions of interest of the same color and drawn on (**a**). 13 μM forskolin (FSK) was applied in the bath for the duration indicated by the bar on the graph. (**c**) Pseudocolor images in control condition (*a*), in the presence of 13 μM forskolin (*b*) and after recovery (*c*). The calibration square indicates fluorescence intensity horizontally and F535/F480 ratio vertically

so there is no need for misregistration correction; (2) for each data point, a stack of images is recorded on a thickness of up to 50 μm at 0.5 μm intervals; and (3) corrections for preparation movements are applied to the *X*, *Y and Z* dimensions, thereby correcting for possible focus drift.

While wide-field images are intrinsically fuzzy (Fig. 5a), two-photon microscopy provides much sharper images (Fig. 5a) allowing for the measurement in specific subcellular domains such as dendritic branches and even spines (Fig. 5c). With this improved spatial resolution, the response to receptor activation can be monitored specifically over the somatic cytosol (Fig. 6) as well as within thin dendritic branches (Fig. 7).

3.9 Response Quantification

The basal ratio is often quite variable from cell to cell, and this variability is generally observed with the control biosensor which is insensitive to the biological signal of interest (Fig. 2). This suggests that some yet to be determined effect influences the biosensor optical properties, including the maturation of the chromophore [16] and absolute calibration of ratio values is therefore impossible at the present time. The ratio response must therefore be calibrated between the Rmin and Rmax values, as originally described for calcium dyes [9] and later adapted for cAMP biosensors [31].

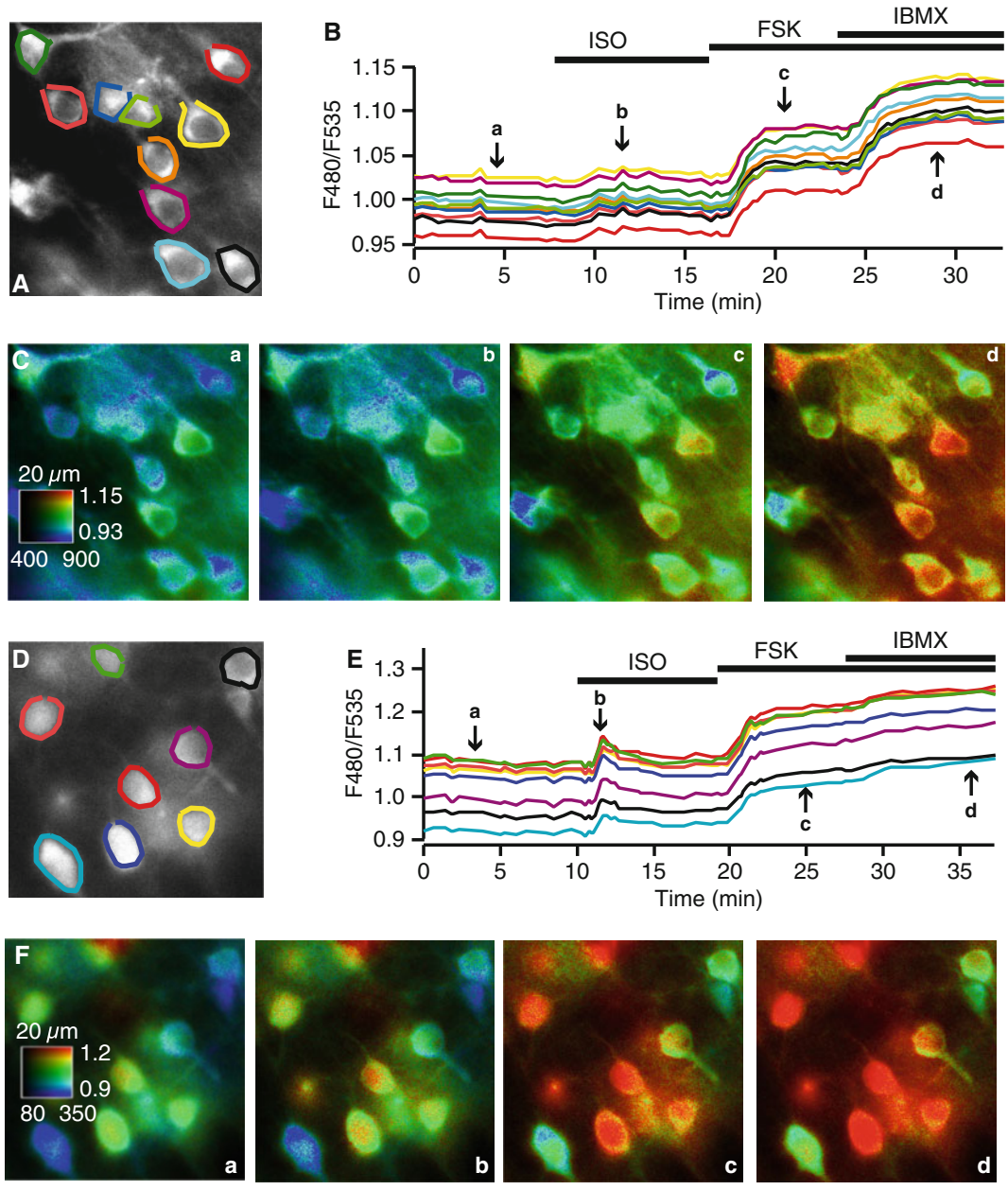

Fig. 4 Monitoring changes in cAMP concentration in response to β-adrenergic stimulation with Epac1-camps and the more sensitive Epac2-camps300 using wide-field microscopy. (**a**, **d**), Wide-field fluorescence images of brain slices expressing Epac1-camps (**a**) and Epac2-camps300 (**d**) at the 535 nm emission wavelength. (**b**, **e**), Each trace indicates the F480/F535 emission ratio measured on the regions indicated by the color contour drawn on the pseudocolor images. 100 nM isoproterenol (ISO), 13 μM forskolin (FSK) and 200 μM IBMX were applied in the bath for the period of time indicated by the bars. (**c**, **f**), Pseudocolor images presenting fluorescence emission ratios indicative of changes in cAMP concentration, as measured with Epac1-camps (**c**) and Epac2-camps300 (**f**) in control condition (*a*), in the presence of isoproterenol (*b*), forskolin (*c*), and forskolin + IBMX (*d*)

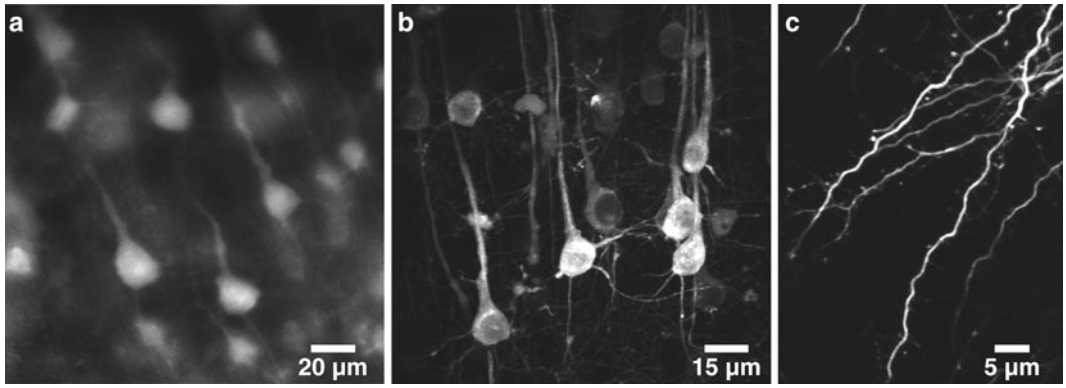

Fig. 5 Fluorescence images of cortical brain slices expressing AKAR2.2 at the 535 nm emission wavelength recorded (**a**) by wide-field microscopy, (**b**) by two-photon microscopy. (**c**) High resolution imaging of the thin dendrites and dendritic spines by two-photon microscopy

3.10 Improved Biosensors for the cAMP/PKA Signaling Cascade

AKAR2.2 was the first biosensor to be routinely used in brain slice preparations, as it provided sizable ratio changes that were reversible on the time-scale of an experiment. This sensor was later improved by replacing the citrine acceptor with a cpVenus, producing AKAR3 with a larger maximal ratio change (Fig. 8) [19]. Further improvement of this biosensor was obtained by changing the CFP donor into a cerulean, having less bleaching and even larger ratio change [20]. This AKAR4 biosensor, as well as other new similar constructs [32], has not yet been tested in brain slices.

An improved version of the cAMP sensor, $^{T}Epac^{VV}$, with an amazing 80 % ratio change has also been released recently but to our knowledge has not yet been tested in brain slices [15].

Further development in the field of biosensor development will undoubtedly change the landscape of biosensor imaging with improved signal resolution in space and time, thereby opening new windows on the amazing complexity of intracellular signal integration in neurons.

4 Notes

1. There are various recipes for the cutting buffer, which would maintain the neurons in better shape, containing kynurenate, lower sodium, etc. The precise recipe used for an experiment may depend on the brain region and should be tested and optimized for each brain region.
2. Although brain slices from young animals are more transparent and have a higher infection rate, both conditions that are favorable for imaging, it is still possible to do imaging on slices from adult rodents.

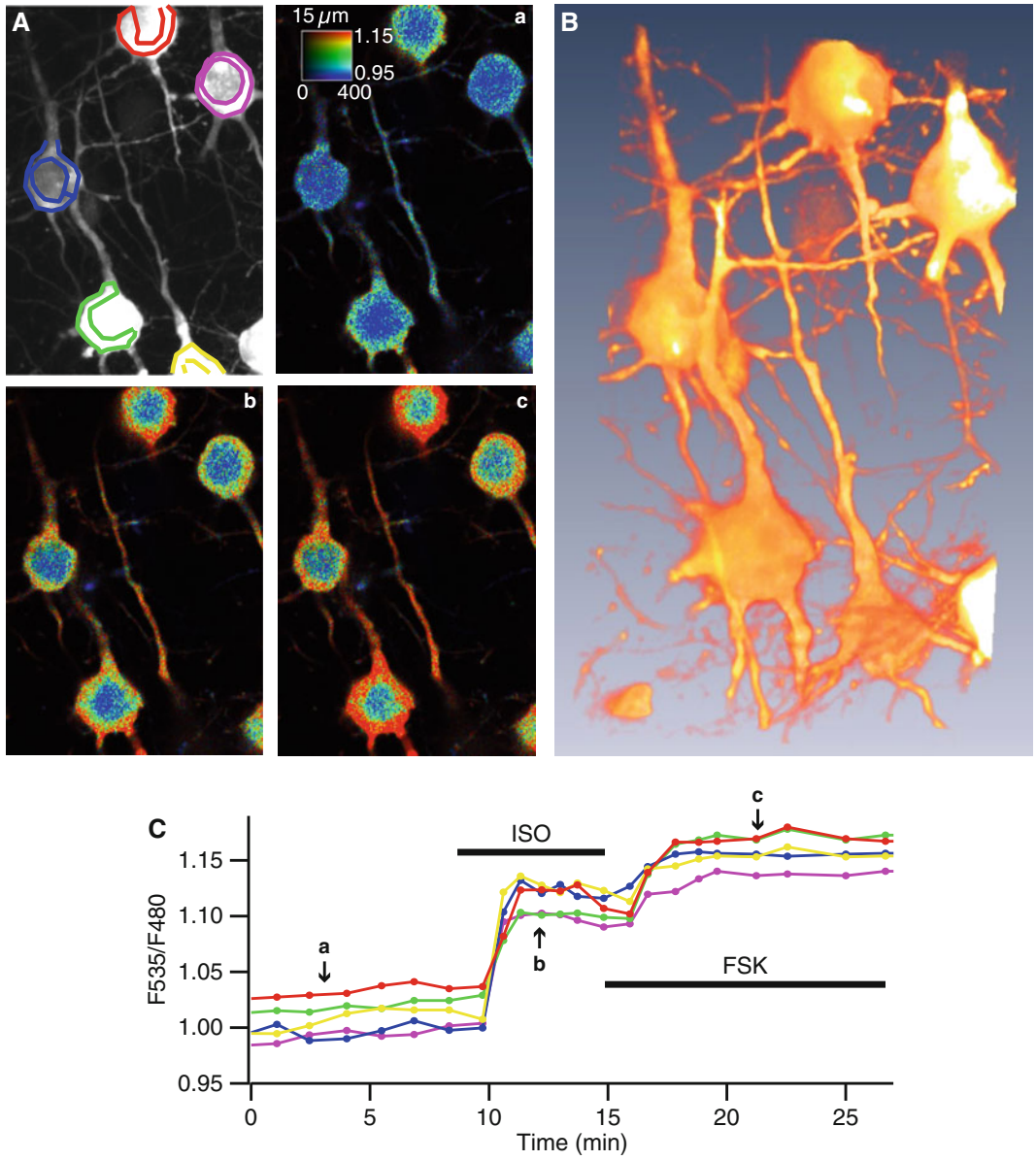

Fig. 6 Monitoring PKA signaling in the soma of cortical neurons expressing AKAR2.2 by two-photon microscopy. (**a**) *Top left*: vertical projection of the brain slice image stack (20 μm thick, 0.5 μm interval) recorded at the 535 emission wavelength. Pseudocolor images in control condition (*a*), in the presence of 100 nM isoproterenol (*b*) and in the presence of 13 μM forskolin (*c*). (**b**) 3D visualization of the image stack (**c**) Ratio values during the course of the recording, measured over the somatic cytosol of the cells. The nucleus, which has different response kinetics, was excluded from the measurement. Each trace corresponds to the cell selected by the region of interest of the same color and drawn on (**a**). *Arrows* indicate the time corresponding to the images in (**a**). 100 nM isoproterenol (ISO) and 13 μM forskolin (FSK) were applied in the bath for the durations indicated by the bars

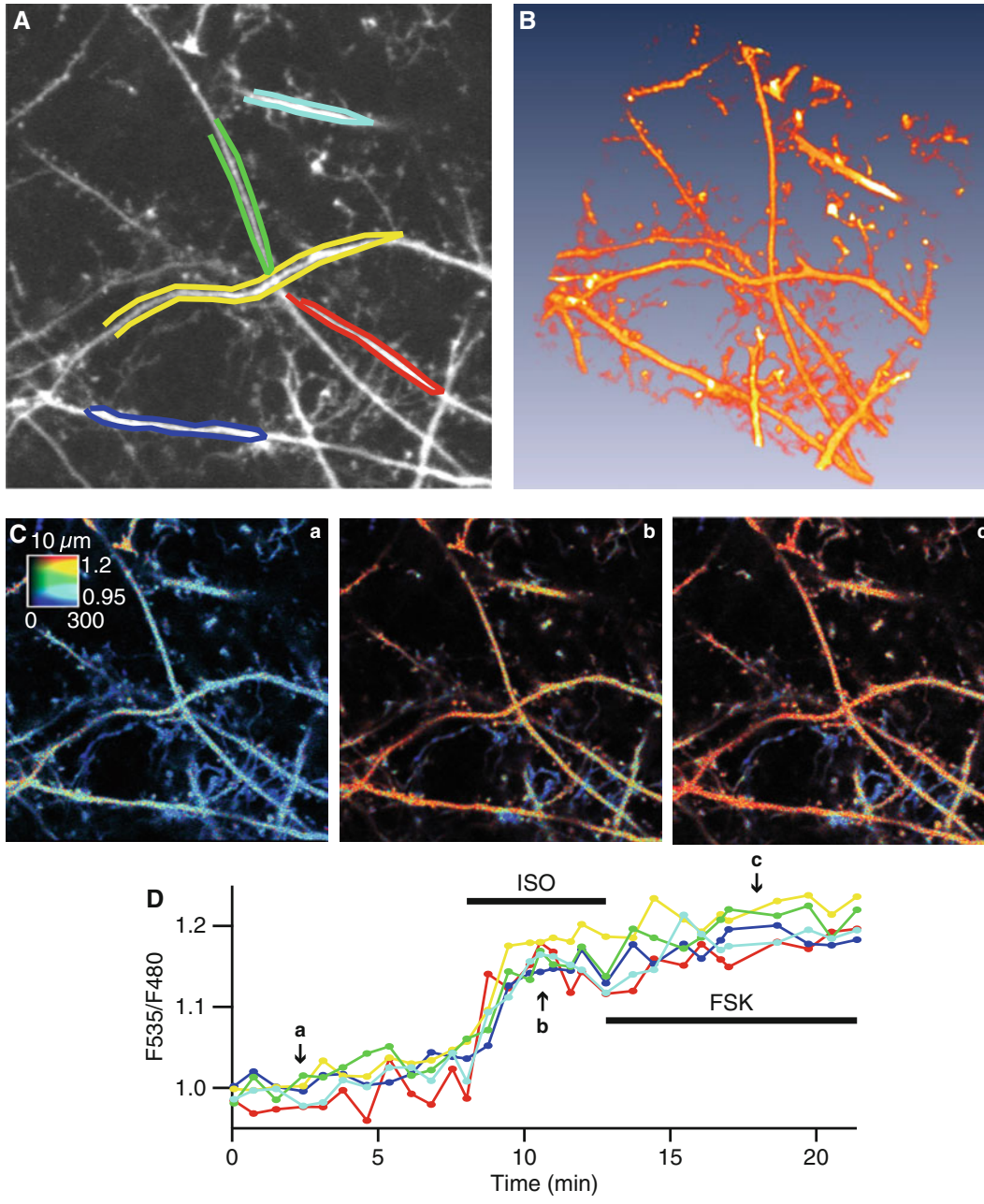

Fig. 7 AKAR2.2 response measured in thin dendrites of cortical neurons by two-photon microscopy. (**a**) Vertical projection of the brain slice image stack (8 μm thick, 0.5 μm interval) recorded at 535 nm emission wavelength. (**b**) 3D visualization of the image stack (**c**) Pseudocolor images in control condition (*a*), in the presence of 100 nM isoproterenol (*b*) and in the presence of 13 μM forskolin (*c*). (**d**) Ratio values during the course of the recording, measured on the regions indicated by the color contour on the grayscale image in (**a**). *Arrows* indicate the time corresponding to the images in (**a**). 100 nM isoproterenol (ISO) and 13 μM forskolin (FSK) were applied in the bath for the durations indicated by the bars

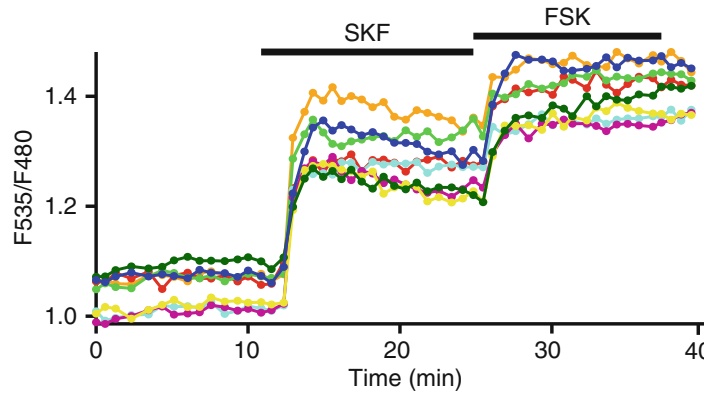

Fig. 8 Improved biosensors result in much larger signal over noise ratio. AKAR3 was expressed in a cortical brain slice. Each trace corresponds to the ratio values during the course of the recording, measured on the soma of individual neurons. 1 μM SKF and 13 μM forskolin (FSK) were applied in the bath for the period of time indicated by the bars. The response amplitude is larger than the similar experiment shown in Fig. 6

3. Bleaching of the biosensor may dramatically limit the experiment. Therefore, unnecessary illumination of the biosensor should be avoided. Below we have listed some common sources of useless damage to the fluorophores:
   (a) Excessively high illumination power: epifluorescence imaging is performed quite well with a 100 W halogen light source, which is sufficient to distinguish the cells by eye and is very stable for quantitative imaging. Illumination that is too strong, such as arc lamps that are used improperly (i.e., without correct attenuation), can bleach the fluorophores and suppress the ratio change. An indication of this phenomenon is a rapid drift of the ratio baseline as a function of the cumulated illumination duration, associated with very small ratio responses.
   (b) Poor illumination control: the light path used for epifluorescence must be electronically controlled by a fast shutter, only allowing illumination of the preparation when acquiring images.
   (c) Too strong transillumination while looking at the biological sample: simply put a yellow tainted glass in the transillumination light path in order to prevent bleaching by the blue component of the transillumination light.
4. Shading images are images of a uniformly fluorescent object, such as a fluorescent solution placed in a hemocytometer. Coumarin 343 (100 μM) is convenient because it emits in both CFP and YFP channels. Since the nonuniformity of the field may be slightly different for the two channels, a shading

image is acquired for each detection channels. Data images are divided by the shading image of the corresponding wavelength, which serves two purposes. First, dividing the acquired image by the shading image corrects for the nonuniformity of the imaging system, usually the center of the image being brighter than the edges. This correction is sometimes called flat-field correction. Shading correction serves a second purpose, as well: since the images from each channel are divided by their respective shading, by definition, the ratio of the shading solution equals 1. Shading correction thus defines the ratio value of 1 as equal to the ratio measured for the specific shading chromophore (Coumarin 343, in our case) which can thus be used to roughly compare ratio values across different imaging setups.

5. It has now been widely reported (although not explained) that brain slices survive better at 35 °C than at 37 °C. A specific incubator should be dedicated to this temperature. Infections also succeeded at room temperature when performed directly inside a 100 ml beaker. In this case, the solution level should be adjusted so that the slices are held on a mesh close to the surface, at the interface with air just for the duration of the infection (30 min), then later submerged again and kept overnight, with continuous gassing with 95 % O_2/5 % CO_2.
6. Drifts of the baseline ratio are sometimes observed during the course of the experiment. This effect can also be observed with AKARmut, showing an effect independent of phosphorylation events, possibly reflecting changes in chromophore properties. Since this effect was reduced when the slices were pre-incubated in the recording medium for ~1 h, it is suspected to result from changes in pH or chloride concentration, which eventually stabilize in the recording solution.
7. During the course of the experiment, the biological object often moves as a result of mechanical instability of the microscope or intrinsic movements of the biological object. A brain slice typically moves by tens of microns, both horizontally and vertically. While the vertical movement must be corrected by adjusting the focus of the microscope, horizontal translations are easy to correct using software, translating the acquired image until it is registered with a reference image. Both image registration and translation are calculated automatically using built-in Igor Pro routines [33].
8. Since all microscopes exhibit some level of chromatic aberration (objective, filter thickness and wedge effect), it is often necessary to register the images from the two channels at the sub-pixel level. This correction is usually determined once for an imaging system and applied to all images acquired on this system.

9. The color of each pixel is coded in tridimensional space and we use the "hue-saturation-value" coding, representing the ratio with a hue from blue to red, and the fluorescence level with the intensity [26]. Saturation is set to 100 %. This results in more "natural looking" images, with the most intense regions of the image appearing bright, and the image gradually fading into darker hues and eventually black as the fluorescence intensity in the original image declines towards background. This display mode thus avoids the artificial thresholding of images which show arbitrary sharp edges.
10. The ratio is evaluated as a weighted average: each pixel in the region of interest is weighted by the intensity of the fluorescence [26]. As a consequence, bright pixels, corresponding to regions of the image containing a large amount of biosensor will contribute more to the average than dim pixels where the biosensor is scarce. This has the advantage that background pixels accidentally contained within a region of interest will be cancelled-out in the average. When fluorescence intensity is close to background, the ratio converges towards "0/0" and values can randomly reach arbitrary values from $-\infty$ to $+\infty$. To remove these infinite values, all ratio values are cropped from $0.1 \times R_{min}$ to $10 \times R_{max}$.
11. The cell to cell differences in the ratio value observed with this control biosensor indicate that different cells "process" the biosensor differently. Sometimes, aggregates where the ratio value is maximal can be seen in the cytosol and demonstrates that rough absolute ratio values cannot be used to evaluate basal cAMP concentrations or PKA phosphorylation levels. The ratio response must be evaluated compared to the R_{min} and R_{max} determined experimentally for each cell.

References

1. Tasken K, Aandahl EM (2004) Localized effects of cAMP mediated by distinct routes of protein kinase A. Physiol Rev 84:137–167
2. Neves SR, Tsokas P, Sarkar A, Grace EA, Rangamani P, Taubenfeld SM, Alberini CM, Schaff JC, Blitzer RD, Moraru II, Iyengar R (2008) Cell shape and negative links in regulatory motifs together control spatial information flow in signaling networks. Cell 133:666–680
3. Adams SR, Harootunian AT, Buechler YJ, Taylor SS, Tsien RY (1991) Fluorescence ratio imaging of cyclic AMP in single cells. Nature 349:694–697
4. Bacskai BJ, Hochner B, Mahaut-Smith M, Adams SR, Kaang BK, Kandel ER, Tsien RY (1993) Spatially resolved dynamics of cAMP and protein kinase A subunits in Aplysia sensory neurons. Science 260:222–226
5. Hempel CM, Vincent P, Adams SR, Tsien RY, Selverston AI (1996) Spatio-temporal dynamics of cyclic AMP signals in an intact neural circuit. Nature 384:166–169
6. Vincent P, Brusciano D (2001) Cyclic AMP imaging in neurones in brain slice preparations. J Neurosci Methods 108:189–198
7. Miyawaki A, Llopis J, Heim R, McCaffery JM, Adams JA, Ikura M, Tsien RY (1997) Fluorescent indicators for Ca2+ based on green fluorescent proteins and calmodulin. Nature 388:882–887
8. Romoser VA, Hinkle PM, Persechini A (1997) Detection in living cells of Ca2+-dependent

changes in the fluorescence emission of an indicator composed of two green fluorescent protein variants linked by a calmodulin-binding sequence. A new class of fluorescent indicators. J Biol Chem 272:13270–13274

9. Grynkiewicz G, Poenie M, Tsien RY (1985) A new generation of Ca2+ indicators with greatly improved fluorescence properties. J Biol Chem 260:3440–3450
10. Zhang J, Campbell RE, Ting AY, Tsien RY (2002) Creating new fluorescent probes for cell biology. Nat Rev Mol Cell Biol 3: 906–918
11. Dulla C, Tani H, Okumoto S, Frommer WB, Reimer RJ, Huguenard JR (2008) Imaging of glutamate in brain slices using FRET sensors. J Neurosci Methods 168:306–319
12. Hires SA, Zhu Y, Tsien RY (2008) Optical measurement of synaptic glutamate spillover and reuptake by linker optimized glutamate-sensitive fluorescent reporters. Proc Natl Acad Sci U S A 105:4411–4416
13. Laxman B, Hall DE, Bhojani MS, Hamstra DA, Chenevert TL, Ross BD, Rehemtulla A (2002) Noninvasive real-time imaging of apoptosis. Proc Natl Acad Sci U S A 99:16551–16555
14. Ai HW, Hazelwood KL, Davidson MW, Campbell RE (2008) Fluorescent protein FRET pairs for ratiometric imaging of dual biosensors. Nat Methods 5:401–403
15. Klarenbeek JB, Goedhart J, Hink MA, Gadella TW, Jalink K (2011) A mTurquoise-based cAMP sensor for both FLIM and ratiometric read-out has improved dynamic range. PLoS One 6:e19170
16. van der Krogt GN, Ogink J, Ponsioen B, Jalink K (2008) A comparison of donor-acceptor pairs for genetically encoded FRET sensors: application to the Epac cAMP sensor as an example. PLoS One 3:e1916
17. Vincent P, Gervasi N, Zhang J (2008) Real-time monitoring of cyclic nucleotide signaling in neurons using genetically encoded FRET probes. Brain Cell Biol 36:3–17
18. Zhang J, Hupfeld CJ, Taylor SS, Olefsky JM, Tsien RY (2005) Insulin disrupts beta-adrenergic signalling to protein kinase A in adipocytes. Nature 437:569–573
19. Allen MD, Zhang J (2006) Subcellular dynamics of protein kinase A activity visualized by FRET-based reporters. Biochem Biophys Res Commun 348:716–721
20. Depry C, Allen MD, Zhang J (2011) Visualization of PKA activity in plasma membrane microdomains. Mol Biosyst 7:52–58
21. Gervasi N, Hepp R, Tricoire L, Zhang J, Lambolez B, Paupardin-Tritsch D, Vincent P (2007) Dynamics of protein kinase A signaling at the membrane, in the cytosol, and in the nucleus of neurons in mouse brain slices. J Neurosci 27:2744–2750
22. Hu E, Demmou L, Cauli B, Gallopin T, Geoffroy H, Harris-Warrick RM, Paupardin-Tritsch D, Lambolez B, Vincent P, Hepp R (2011) VIP, CRF, and PACAP Act at distinct receptors to elicit different cAMP/PKA dynamics in the Neocortex. Cereb Cortex 21: 708–718
23. Castro LR, Gervasi N, Guiot E, Cavellini L, Nikolaev VO, Paupardin-Tritsch D, Vincent P (2010) Type 4 phosphodiesterase plays different integrating roles in different cellular domains in pyramidal cortical neurons. J Neurosci 30:6143–6151
24. Ehrengruber MU, Lundstrom K, Schweitzer C, Heuss C, Schlesinger S, Gahwiler BH (1999) Recombinant Semliki Forest virus and Sindbis virus efficiently infect neurons in hippocampal slice cultures. Proc Natl Acad Sci U S A 96:7041–7046
25. Nguyen QT, Tsai PS, Kleinfeld D (2006) MPScope: a versatile software suite for multiphoton microscopy. J Neurosci Methods 156: 351–359
26. Tsien RY, Harootunian AT (1990) Practical design criteria for a dynamic ratio imaging system. Cell Calcium 11:93–109
27. DiPilato LM, Cheng X, Zhang J (2004) Fluorescent indicators of cAMP and Epac activation reveal differential dynamics of cAMP signaling within discrete subcellular compartments. Proc Natl Acad Sci U S A 101: 16513–16518
28. Nikolaev VO, Bunemann M, Hein L, Hannawacker A, Lohse MJ (2004) Novel single chain cAMP sensors for receptor-induced signal propagation. J Biol Chem 279: 37215–37218
29. Ponsioen B, Zhao J, Riedl J, Zwartkruis F, van der Krogt G, Zaccolo M, Moolenaar WH, Bos JL, Jalink K (2004) Detecting cAMP-induced Epac activation by fluorescence resonance energy transfer: Epac as a novel cAMP indicator. EMBO Rep 5:1176–1180
30. Norris RP, Ratzan WJ, Freudzon M, Mehlmann LM, Krall J, Movsesian MA, Wang H, Ke H, Nikolaev VO, Jaffe LA (2009) Cyclic GMP from the surrounding somatic cells regulates cyclic AMP and meiosis in the mouse oocyte. Development 136:1869–1878
31. Börner S, Schwede F, Schlipp A, Berisha F, Calebiro D, Lohse MJ, Nikolaev VO (2011) FRET measurements of intracellular cAMP concentrations and cAMP analog permeability in intact cells. Nat Protoc 6:427–438

32. Komatsu N, Aoki K, Yamada M, Yukinaga H, Fujita Y, Kamioka Y, Matsuda M (2011) Development of an optimized backbone of FRET biosensors for kinases and GTPases. Mol Biol Cell 22:4647–4656

33. Thevenaz P, Ruttimann UE, Unser M (1998) A pyramid approach to subpixel registration based on intensity. IEEE Trans Image Process 7:27–41